



HAL
open science

Comparative Description of the Microwave Surface Impedance of Nb, BaKBiO, and YBaCuO

A. Golubov, M. Trunin, A. Zhukov, O. Dolgov, S. Shulga

► **To cite this version:**

A. Golubov, M. Trunin, A. Zhukov, O. Dolgov, S. Shulga. Comparative Description of the Microwave Surface Impedance of Nb, BaKBiO, and YBaCuO. *Journal de Physique I*, 1996, 6 (12), pp.2275-2290. 10.1051/jp1:1996217 . jpa-00247311

HAL Id: jpa-00247311

<https://hal.science/jpa-00247311>

Submitted on 4 Feb 2008

HAL is a multi-disciplinary open access archive for the deposit and dissemination of scientific research documents, whether they are published or not. The documents may come from teaching and research institutions in France or abroad, or from public or private research centers.

L'archive ouverte pluridisciplinaire **HAL**, est destinée au dépôt et à la diffusion de documents scientifiques de niveau recherche, publiés ou non, émanant des établissements d'enseignement et de recherche français ou étrangers, des laboratoires publics ou privés.

Comparative Description of the Microwave Surface Impedance of Nb, BaKBiO, and YBaCuO

A.A. Golubov (¹), M.R. Trunin (^{1,*}), A.A. Zhukov (¹), O.V. Dolgov (²)
and S.V. Shulga (³)

(¹) Institute of Solid State Physics, 142432 Chernogolovka, Moscow district, Russia

(²) P.N. Lebedev Physical Institute, Moscow, Russia

(³) Institute of Spectroscopy, Troitsk, Russia

(Received 23 April 1996, accepted 3 June 1996)

PACS.74.20.Fg – BCS theory and its development

PACS.75.25.Nf – Response to electromagnetic fields (nuclear magnetic resonance, surface impedance, etc.)

Abstract. — Measurements of microwave impedance *versus* temperature, $Z_s(T)$, in Nb, Ba_{0.6}K_{0.4}BiO₃, and YBa₂Cu₃O_{7- δ} are given. The measurements were made by the “hot finger” cavity perturbation technique. The electromagnetic properties of Nb are in a good quantitative agreement with the isotropic s-wave BCS theory. This model can also describe the experimental $Z_s(T)$ curves in Ba_{0.6}K_{0.4}BiO₃ crystals if the nonhomogeneous broadening of the superconducting transition is properly taken into account. The behavior of the microwave impedance of YBa₂Cu₃O_{7- δ} disagrees with the isotropic BCS theory. This suggests a strong anisotropy of the order parameter in this compound. Since the controversy between s- and d-wave descriptions of YBa₂Cu₃O_{7- δ} properties has not been resolved yet, we have checked a simpler strongly anisotropic s-wave model. Calculations by this model have been compared to measurements on YBa₂Cu₃O_{7- δ} . With due account of the strong-coupling effects, two-band anisotropy, and impurity scattering in YBa₂Cu₃O_{7- δ} , the agreement between the generalized BCS model and experimental data is surprisingly good.

1. Introduction

Given measurements of the microwave impedance *versus* temperature, $Z_s(T) = R_s(T) + iX_s(T)$, at a microwave frequency $\omega/2\pi \sim 10$ GHz, one can derive quite straightforwardly the superconducting gap width $\Delta(T)$, penetration depth of electromagnetic field $\lambda(T)$, impurity scattering rate in a superconductor, and, as a result of a more complex analysis, the superconducting pairing mechanism. In the local electrodynamics, which can be applied to experiments discussed in the paper, a simple relation exists between the surface resistance R_s and reactance X_s of a superconductor, on one hand, and its complex conductivity, $\sigma_s = \sigma_1 - i\sigma_2$, on the other hand:

$$Z_s = R_s + iX_s = \left(\frac{i\omega\mu_0}{\sigma_1 - i\sigma_2} \right)^{1/2} \quad (1)$$

(*) Author for correspondence (e-mail: trunin@issp.ac.ru)

Equation (1) yields the expressions for the real and imaginary parts of the conductivity in terms of the measurable quantities R_s and X_s :

$$\sigma_1 = \frac{2\omega\mu_0 R_s X_s}{(R_s^2 + X_s^2)^2}, \quad \sigma_2 = \frac{\omega\mu_0 (X_s^2 - R_s^2)}{(R_s^2 + X_s^2)^2}. \quad (2)$$

In the low-frequency limit, $\hbar\omega \ll \Delta$, the Bardeen-Cooper-Schrieffer (BCS) theory [1] predicts two distinctive features in T -dependence of the response of a superconductor, namely an exponential drop in $\sigma_s(T)$ and $Z_s(T) \propto \exp(-\Delta(0)/kT)$ in the range $T < 0.5T_c$, and an increase in the conductivity $\sigma_1(T)$ at $T \leq T_c$ with respect to its value σ_n at $T = T_c$. These features are, respectively, due to the thermal activation of normal quasiparticles above the gap $\Delta(T)$ and the singularity in the density of states at a quasiparticle energy equal to $\Delta(T)$. Therefore the BCS model [1] can be directly checked by detecting a maximum in the microwave conductivity $\sigma_1(T)$ in the range of temperatures $T \sim 0.85T_c$ (a so-called coherence peak). This can be done by simultaneous and precision measurements of the absolute values of $R_s(T)$ and $X_s(T)$, as has been performed for the first time quite recently. O. Klein *et al.* [2] have detected a coherence peak in Nb and Pb at a frequency of 60 GHz. The experiment demands samples of a high quality, namely, the superconducting transition width ΔT must be very small ($\Delta T \ll 0.1T_c$), besides, the residual surface resistance, which always contributes to measurements of $R_s(T)$ at $T \rightarrow 0$ because of various defects in the surface layer, should be also small: $R_0 \ll R_s(T_c/2)$.

The generalization of the BCS theory to strong electron-phonon coupling was proposed by Eliashberg [3]. It follows from this theory that for strong enough coupling the singularity in the density of states at $\hbar\omega = \Delta(T)$ is broadened due to inelastic electron scattering by thermally excited phonons. As a result, the coherence peak amplitude decreases with an increase in the electron-phonon coupling constant and completely vanishes at frequencies around 10 GHz [4] if this constant is larger than two. This conclusion from the strong-coupling (SC) model has been confirmed by measurement of the microwave conductivity $\sigma_1(T)$ around T_c in $\text{YBa}_2\text{Cu}_3\text{O}_{7-\delta}$ (YBCO) samples [5–7], whose critical temperature was $T_c \sim 90$ K. The SC model also accounted for the nonexponential behavior of $R_s(T)$ and $\lambda(T)$ in YBCO [8, 9] at $T < T_c/2$.

Microwave measurements of $\lambda(T)$ performed in 1993 on high-quality YBCO samples [10–12], whose residual resistance R_0 was considerably lower than that of previously studied materials, could not be described in terms of the SC model. The main conclusion which can be drawn from the results by Hardy *et al.* [10], Ma *et al.* [11], and N. Klein *et al.* [12] is that the temperature dependence of $\Delta\lambda_{ab}(T)$ in the ab -plane of YBCO at $T < T_c/4$ switches from exponential [12] to linear [10] and quadratic [11] with the increase in R_0 and oxygen deficiency in a sample. Subsequent microwave measurements [13–15] confirmed that the function $\Delta\lambda_{ab}(T)$ was linear, although it seemed quite unusual for the s-wave pairing in a superconductor. Figure 1 shows the low temperature section of the experimental $\Delta\lambda_{ab}(T)$ curve from reference [16], which can be described by neither BCS nor SC models. Another experimental feature observed in YBCO samples with low R_0 is a plateau [11, 12, 14, 15] or even a small peak [13, 15] in the surface resistance $R_s(T)$ around $T_c/2$. This singularity in $R_s(T)$ results in a broad maximum in $\sigma_1(T)$.

The existence of the maximum in $\sigma_1(T)$, as well as the crossover from the linear to quadratic dependence in $\Delta\lambda(T)$, have been demonstrated by calculations using the d-wave pairing model with due account of impurity scattering [17]. Such a crossover was really observed by Bonn *et al.* [13] after doping YBCO samples with Zn. It is impossible, however, to reconcile the d-wave model with the exponential activation behavior of $\Delta\lambda_{ab}(T)$. Moreover, the experimentally observed slope of $\lambda_{ab}^{-2}(T)$ curves around T_c is much larger than that predicted by this model.

Hence the question arises whether a scenario different from the d-wave one can describe all these features of the impedance. The aim of this work is to demonstrate that it is indeed

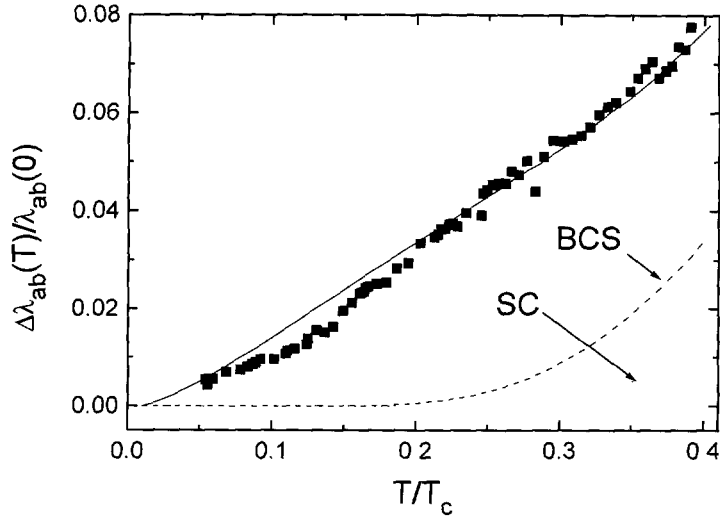


Fig. 1. — Low T section of $\Delta\lambda_{ab}(T)$ vs. T/T_c . Solid labels: data from reference [16]. Solid lines: two-band model with $\gamma_{22}^s = 2.4$ meV, $\gamma_{12} = 0.8$ meV, $\gamma_{11} = \gamma_{22} = 3.2$ meV (see below). Dashed lines: weak coupling BCS model. Dotted lines: isotropic SC model with $\lambda_{11} = 3$.

possible within the strongly anisotropic Eliashberg model. In order to show that, the measurements on Nb, $\text{Ba}_{0.6}\text{K}_{0.4}\text{BiO}_3$ (BKBO), and YBCO samples are compared to the calculations by this model with a proper account of anisotropy, impurity scattering and sample inhomogeneity.

2. Experiment

The “hot finger” cavity perturbation technique originally proposed by Sridhar [18] is most convenient for absolute measurements of $R_s(T)$ and $X_s(T)$ in small superconducting samples. We used a high- Q Nb cavity operating at $T = 4.2$ K resonant at a frequency $f_0 = 9.42$ GHz [19] in the H_{011} mode. A sample was placed at the cavity center in the region of almost uniform microwave magnetic field on an end of a sapphire rod. The entire unit supporting the sample and cavity was in a high vacuum, therefore, given that the rod was thermally insulated, the sample temperature could be tuned over a wide range without heating the cavity.

Measurements of two Nb and BKBO samples of nearly cubic shape with a volume of ~ 1 mm³ are given as an example. The BKBO sample was manufactured by the electrochemical growth technique [20]. It is interesting to compare BKBO and Nb because both materials have cubic structures and are isotropic superconductors whose critical temperatures differ by a factor of three. Therefore it seems natural to try to interpret their superconducting properties in terms of the BCS [1] or SC [3] models. The issue of the applicability of these models to BKBO has not been resolved because BKBO parameters derived from experimental data by different authors [21–24] vary considerably. Moreover, several anomalous properties of BKBO have been observed in both normal and superconducting states, such as positive curvature of the second critical field plotted against temperature [25]. No microwave measurements of the surface impedance in BKBO crystals have been reported by now.

Figures 2 and 3 show parameters measured in experiments, namely the Q -factor of the cavity with the Nb (Fig. 2) and BKBO (Fig. 3) samples and changes in the resonant frequency $\Delta f(T) - \Delta f_0(T)$, where $\Delta f_0 \ll \Delta f$ is the frequency variation of the empty cavity, as functions

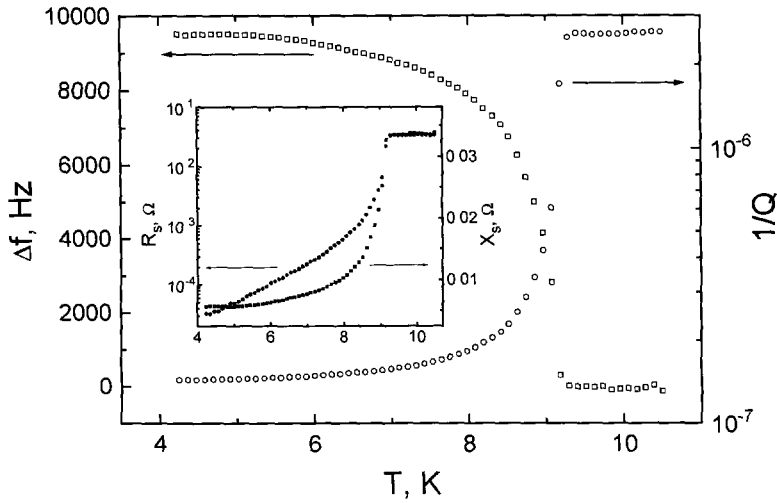


Fig. 2. — Temperature dependences of $1/Q$ (open circles) and frequency shift Δf (open squares) of Nb. Inset: real R_s (solid circles) and imaginary X_s (solid squares) parts of the surface impedance of Nb.

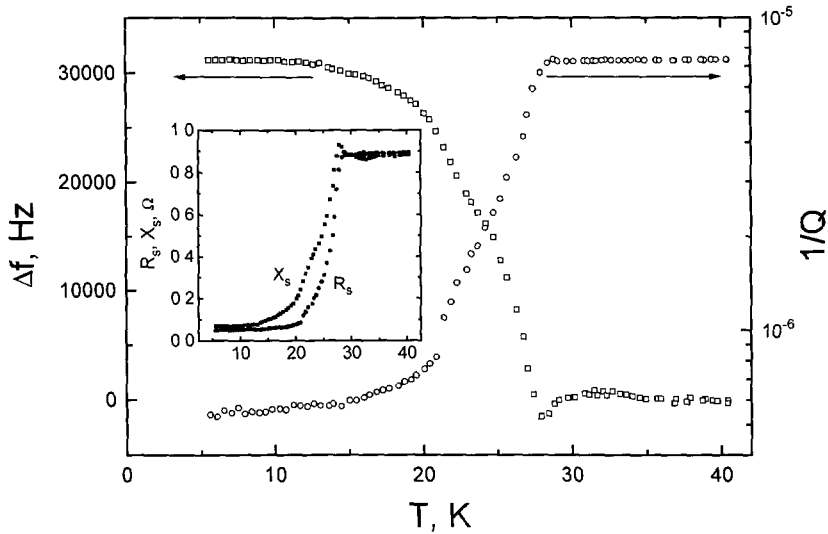


Fig. 3. — Temperature dependences of $1/Q$ (open circles) and frequency shift Δf (open squares) of BKBO. Inset: real R_s (solid circles) and imaginary X_s (solid squares) parts of the surface impedance of BKBO crystal.

of temperature. The uncertainties of our measurements were $\delta(1/Q) \sim 10^{-9}$ and $\delta f_0 \sim 10$ Hz. The temperature dependence of the surface impedance, Z_s (*i.e.*, the surface resistance R_s and the reactance X_s) was derived from Q and Δf using the relations:

$$R_s(T) = \Gamma_s [Q^{-1}(T) - Q_0^{-1}(T)], \quad X_s(T) = -\frac{2\Gamma_s}{f_0} [\Delta f(T) - \Delta f_0(T)] + X_0 \quad (3)$$

where Γ_s is the geometric factor of the sample and X_0 is a fitting parameter. The properties of our samples could be described in the skin-depth limit in the normal state, and we have used the relation $R_n = X_n$, which holds above T_c , to determine X_0 . In order to determine Γ_s of Nb or BKBO samples, we compared the measured normal state microwave loss $R_s(T \geq T_c)$ to the calculation of $R_n = \sqrt{\omega\mu_0\rho/2}$ derived from independent measurements of the dc resistivity ρ .

The inset to Figure 2 shows the curves of $R_s(T)$ and $X_s(T)$ for the Nb sample. In the normal state ($T \geq T_c = 9.2$ K), $R_n = X_n \approx 33$ m Ω , which corresponds to $\rho(T_c) \approx 3$ $\mu\Omega$ cm and the carrier relaxation time $\tau \approx 2 \times 10^{-14}$ s. The surface resistance drops by a factor of 1000 as the temperature changes from T_c to $T_c/2$. At temperatures below 5 K, the surface reactance is constant at $X_s(T) \approx X_s(0) \approx 6$ m Ω .

The inset of Figure 3 shows curves of $R_s(T)$ and $X_s(T)$ for the BKBO sample. They are notably different from similar curves for Nb. Firstly, when the temperature drops from $T = T_c \approx 29$ K to $T = 5$ K, the surface resistance $R_s(T)$ changes only by a factor of 18 and is almost constant at $R_0 \approx 49$ m Ω as $T \rightarrow 0$. Secondly, the superconducting transition is wide and its shape is unusual: it seems that it consists of two sequential transitions, the first one starting at $T \approx 29$ K, the second one at $T \approx 26$ K. They are also seen on the curves of $1/Q$ and Δf versus temperature in Figure 3. A similar shape of the superconducting transition was recorded earlier in measurements of the magnetization of BKBO samples with a record low resistivity $\rho(40$ K) < 100 $\mu\Omega$ cm [25]. Our sample is contaminated more heavily: its resistance $R_s(40$ K) ≈ 0.89 Ω corresponds to a resistivity $\rho(40$ K) ≈ 2100 $\mu\Omega$ cm and $\tau \approx 0.5 \times 10^{-14}$ s.

3. Complex Conductivity and Microscopic Scale Disorder in the BCS and SC Models

Given absolute measurements of $R_s(T)$ and $X_s(T)$, we can calculate the real and imaginary parts of the conductivity $\sigma_1(T)$ and $\sigma_2(T)$ from equation (2) and compare them to theoretical curves. General expressions for the electromagnetic response of a superconductor in the isotropic BCS and SC models were given by Nam [26]. Assuming the dirty limit, $l < \xi_0$, where l is the mean free path and ξ_0 is the coherence length, applicable to our samples, and weak coupling regime, one can easily derive an exact formula for σ_2/σ_n from reference [26]:

$$\frac{\sigma_2}{\sigma_n} = \frac{\pi\Delta(T)}{\hbar\omega} \tanh\left(\frac{\Delta}{kT}\right), \quad (4)$$

where σ_n is the normal state conductivity, and an approximate formula for σ_1/σ_n :

$$\frac{\sigma_1}{\sigma_n} \approx \frac{\Delta(T)}{2kT} \cosh^{-2}\left(\frac{\Delta}{2kT}\right) \ln\left(\frac{\Delta}{\hbar\omega}\right). \quad (5)$$

The coherence peak is due to the logarithmic cofactor on the right of equation (5). The peak amplitude drops with an increase in the electron-phonon coupling constant. Inset to Figure 4 from reference [6] shows the difference between the curves of $\sigma_1(T)$ derived from the isotropic BCS and SC models. The calculations have been done with the coupling constant equal to 2 in order to interpret the measurements of $\sigma_1/\sigma_n(T/T_c)$ in YBCO at a frequency of 3 GHz, which are shown by the dashed line in Figure 4.

The circles in Figure 5 show the ratio σ_1/σ_n for Nb derived from measurements of R_s and X_s using equation (2) (Fig. 2). The solid line shows the function $\sigma_1/\sigma_n(T/T_c)$ calculated using the equations from reference [26], the BCS model with $\Delta(0) = 1.76kT_c$ and previously known ω and τ . Figure 5 also shows the experimental (squares) and theoretical (solid curve) London

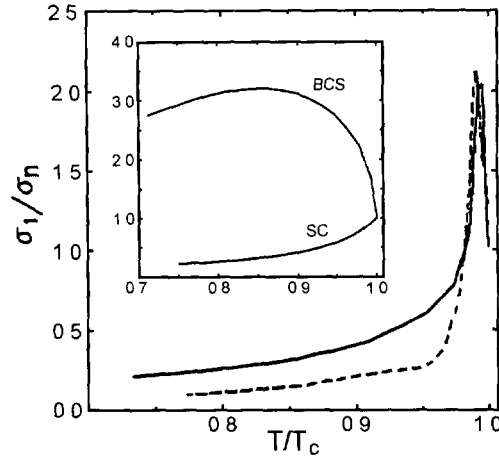


Fig. 4. — Comparison of the experimental data (dashed line, YBCO) for σ_1/σ_n and of the results of calculations within the SC model with account for sample inhomogeneity (solid line). Inset: temperature dependence of σ_1/σ_n calculated in the framework of the BCS model and SC model (Ref. [6])

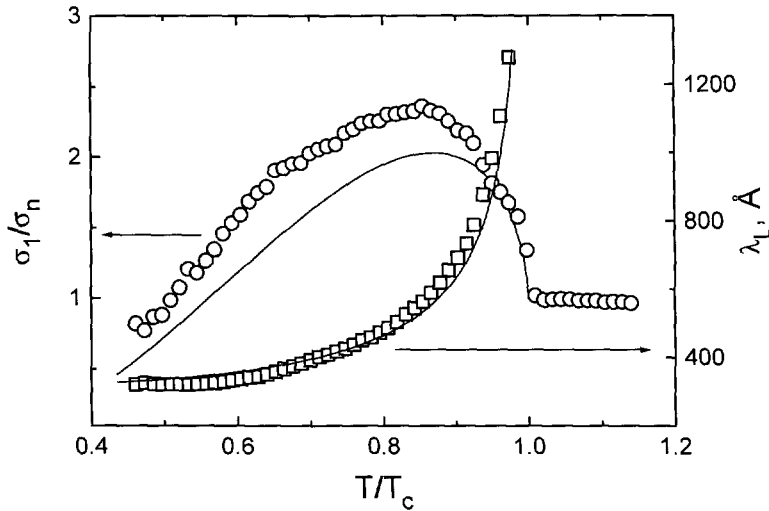


Fig. 5. — Real part of the microwave conductivity normalised to that in normal state σ_1/σ_n (open circles) and the London penetration depth λ_L (open squares) *vs.* normalised temperature T/T_c for Nb (see Fig. 2). Solid lines: σ_1/σ_n and λ_L calculated by the BCS model.

penetration depth of magnetic field *versus* temperature, $\lambda_L(T)$, for Nb. In the dirty limit $\lambda_L(0)$ is related to the measured parameter $\lambda(0) = X_s(0)/\omega\mu_0$ through the equation

$$\lambda_L(0) = \lambda(0)\sqrt{l/\xi_0} = \lambda(0)\sqrt{\pi\Delta(0)\tau/\hbar} \quad (6)$$

The resulting value $\lambda_L(0) = 320 \pm 10 \text{ \AA}$ agrees with the literature data for Nb [2,27]. Thus the experimental curves of $Z_s(T)$ in the Nb sample lead us to a certain conclusion that the isotropic BCS model [1,26] applies to the electromagnetic properties of Nb.

In view of the discussed peculiarities of the $Z_s(T)$ curve in BKBO due to defects in the surface layer, it is impossible to compare the details of experimental results in the range around the critical temperature to the theory of reference [26]. Nonetheless, we will demonstrate how the experimental curves of $R_s(T)$ and $X_s(T)$ in Figure 3 can be described in terms of the BCS model taking into account the sample nonhomogeneity and residual loss R_0 . To this end, we use a simple model of effective medium [6], which we had proposed previously to account for a narrow peak in the microwave conductivity $\sigma_1(T)$ in YBCO (Fig. 4).

Assume that different regions of our samples undergo the superconducting transition at different critical temperatures in the interval ΔT_c . If the dimension of each of these regions is smaller than the magnetic field penetration depth (microscopic-scale disorder), the distribution of the microwave current in the sample is uniform, and the effective impedance Z_{eff} is calculated in two steps: first the impedances of all the regions Z_s (with different T_c) connected by a current line are added, then the sum is averaged over the sample volume. As a result, we have

$$Z_{\text{eff}}(T) = \int_{\Delta T_c} Z_s(T, T_c) f(T_c) dT_c \quad (7)$$

where the distribution function $f(T_c)$ is such that the fraction of the sample volume where the critical temperatures belong to the interval $T_c < T < T_c + dT_c$ is $f(T_c)dT_c$. In the simplest case $f(T_c)$ is Gaussian.

The width of the distribution function $f(T_c)$ for the YBCO single crystal with $T_c = 91$ K was selected to be 0.5 K, and the function $Z_s(T, T_c)$ was taken equal to the surface impedance *versus* temperature calculated using the isotropic SC model [6, 26]. The parameters $R_{\text{eff}}(T)$ and $X_{\text{eff}}(T)$ derived from equation (7) were used to calculate $\sigma_{1,\text{eff}}(T)$ by equation (2). The calculations and the experimental curve of $\sigma_1/\sigma_n(T/T_c)$ are compared in the Figure 4, which demonstrates the absence of the BCS coherence peak in YBCO.

As concerns BKBO, the distribution function $f(T_c)$ for different regions of the sample should reflect both observed transitions (Fig. 3). As the temperature increases, the broader low-temperature transition peaking at $T_{c2} \approx 26$ K is followed by the narrow transition with the maximum at $T_{c1} \approx 28$ K.

Figure 6 shows dimensionless parameters

$$r = \frac{R_s - R_0}{R_n - R_0} \approx \frac{R_s - R_0}{R_n}, \quad x = \frac{X_s}{X_n - R_0} \approx \frac{X_s}{R_n} \quad (8)$$

plotted against temperature. The denominator in the equation for r includes only the temperature-dependent part of the surface resistance, which was obtained by subtracting the residual resistance $R_0 \ll R_n$ from the data for $R_s(T)$ in Figure 3. The solid lines show the effective parameters r and x derived using equation (7), where the impedance $Z_s(T, T_c)$ was calculated by the BCS formulas [26] with $\Delta(0) = 1.76kT_c$, and the distribution function was

$$f(T_c) = \frac{2}{3} \left(\frac{2}{\pi} \right)^{1/2} \left[\frac{1}{\Delta T_1} \exp \left(- \frac{(T_{c1} - T)^2}{2\Delta T_1} \right) + \frac{1}{\Delta T_2} \theta(T_{c2} - T) \exp \left(- \frac{(T_{c2} - T)^2}{2\Delta T_2} \right) \right]$$

where $T_{c1} = 28$ K, $\Delta T_1 = 1$ K; $T_{c2} = 26.5$ K, $\Delta T_2 = 4.7$ K. Empty squares in this diagram show the function $\sigma_2/\sigma_n(T/T_c)$ derived from measurements of r and x using equation (2), the solid line shows the effective conductivity $\sigma_{2,\text{eff}}/\sigma_n$ also derived using equation (2), but from the effective parameters r and x , and the dashed curve shows the function defined by equation (4), which is identical to the solid curve at $T < 0.3T_c$. The minimum imaginary part of the impedance is $X_s(0) \approx X_s(5 \text{ K}) \approx 70 \text{ m}\Omega$ (Fig. 3), hence $\lambda(0) = X_s(0)/\omega\mu_0 \approx 9400 \text{ \AA}$.

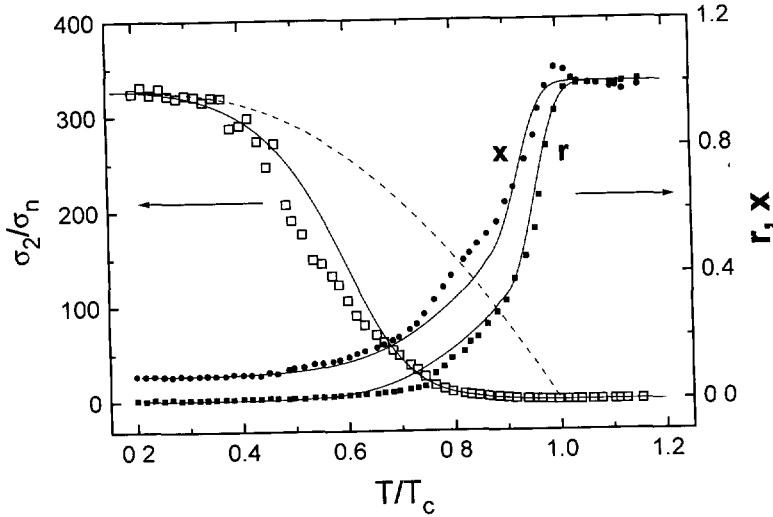


Fig. 6. — Real r (solid squares) and imaginary x (solid circles) parts of the normalised surface impedance, and imaginary part of normalised conductivity σ_2/σ_n (open squares) vs. T/T_c of BKBO sample. Solid lines: effective values of r , x and σ_1/σ_n calculated by the BCS model with the critical temperature distribution function due to inhomogeneities in the sample. Dashed line: data from equation (4).

Taking into account the measurement uncertainty and the factor $\sqrt{l/\xi_0} \approx 0.33$, we derive from equation (6) the London penetration depth in the BKBO sample: $\lambda_L(0) = 3100 \pm 100 \text{ \AA}$. This value agrees with recent measurements of $\lambda(0)$ [28, 29] corrected for the impurity scattering: $\lambda_L(0) = \lambda(0)/\sqrt{1 + \xi_0/l}$.

4. Two-Band Model

In our previous paper [30], we indicated that all recent measurements of the ab -plane penetration depth in YBCO can be described in terms of the s-wave two-band model. This model is a generalization of the SC theory to layered high- T_c cuprates, in particular to YBCO. A strong electron-phonon interaction in the S-band (CuO₂ planes) was assumed, superconductivity in the N-band (CuO chains) being due to interband proximity effect [30–32].

Typical curves of the density of states (DOS) in a two-band superconductor are shown in Figure 7. The behavior of DOS in the S-band is practically the same as in a one-band superconductor with strong electron-phonon interaction. At low and intermediate temperatures, the position of the DOS maximum does not depend on T , only the peak width changes rapidly near T_c . The behavior of DOS in the N-band is quite unusual. The position of the sharp DOS maximum is almost temperature-independent, therefore the low-energy states are filled as the temperature increases, rather than the gap is closed as in the BCS model. The strong temperature dependence of the peak width is due to the strong temperature dependence of the quasiparticle scattering rate. Although a small energy gap exists in the N-band at zero temperature, this gap is easily smeared out by any pair-breaking process, for example by magnetic impurities (see below). These generic properties of the model manifest themselves in the microwave response.

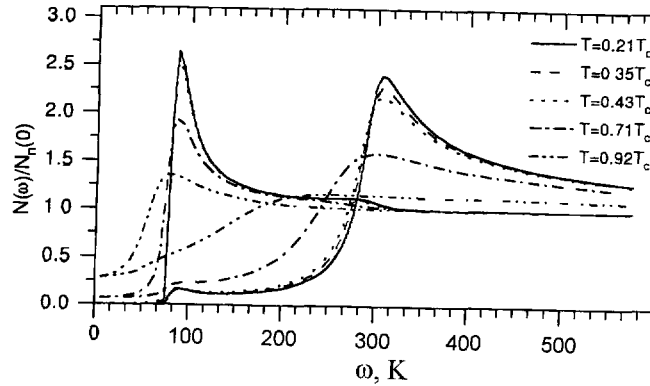


Fig. 7. — Densities of states $N_N(\omega)$ and $N_S(\omega)$ versus temperature (Ref. [33])

In the discussed case of strong pairing in the S-band, the Eliashberg SC theory can be selected as a starting point for discussing the anisotropy effects since this theory properly takes into account the effects of retardation and decay of quasiparticle excitations. The straightforward generalization of the Eliashberg equations for the many-band case leads to a system of coupled Eliashberg equations for the order parameters $\Delta'_{i,n}$ and renormalized quasiparticle energies $\omega'_{i,m}$ in different bands (see, *e.g.* Ref. [30]). These equations include the following parameters: the coupling constants λ_{ij} , the scattering rates γ_{ij} from the i -th to j -th band due to nonmagnetic impurities, and γ_{ij}^s , which is a similar parameter for magnetic impurities.

The choice of parameters in this model is largely controlled by the structure and parameters of YBCO. We assume that the planes are characterized by a large coupling constant and form an S-band ($\lambda_{11} \simeq 3$), whereas the chains form an N-band ($\lambda_{22} = 0$). A nonzero order parameter in the chains is caused by the interband interactions $\lambda_{12} = \lambda_{21} = 0.2$. This set of parameters is consistent with $T_c = 90$ K in YBCO. We have assumed that the interband scattering rates γ_{ij} are small, $\gamma_{12}, \gamma_{21} \ll T_c$, and selected $\gamma_{12}^s = \gamma_{21}^s = \gamma_{11}^s = 0$. We have taken into account impurity scattering due to usual and magnetic impurities in N-band, γ_{22} and γ_{22}^s respectively, and nonmagnetic scattering in S-band γ_{11} .

Given the elastic scattering rates in N and S-band $\gamma_{11} = \gamma_{22} = 2 \div 4 T_c$ (16 ÷ 32 meV), the model is consistent with the absolute values of resistivity at 100 K of about 50 ÷ 100 $\mu\Omega$ cm, as well as with an ab -plane anisotropy of about 2 measured in YBCO.

The cause of magnetic scattering is that at a lower oxygen content, most oxygen atoms are not in the chains. As a result, the chain Cu atoms gain magnetic moments which act as pair breakers. Thus, the magnetic scattering in the N-band γ_{22}^s is the only free parameter of the model related to the oxygen deficiency in $\text{YBa}_2\text{Cu}_3\text{O}_{7-\delta}$.

With the parameters specified above, the Eliashberg equations have been solved numerically for two bands. Figure 8 from reference [30] demonstrates the quantitative comparison of the calculations $\lambda_{ab}^{-2}(T)$ with the single crystal data from references [13, 14] ($\rho_{ab} \simeq 50 \mu\Omega$ cm). A good agreement with the calculations can be seen, except the temperature range close to T_c . The linear dependence in the range $T < 0.5T_c$ is well described by the model. The inset to Figure 8 shows calculations of $\Delta\lambda_{ab}(T)$ for different γ_{22}^s values. As a consequence of the emergence of the gapless state, a crossover from the exponential temperature dependence at low T for $\gamma_{22}^s = 0$ to the linear temperature dependence at larger γ_{22}^s takes place.

With a further increase in γ_{22}^s and γ_{22} , the contribution of the N-band to the penetration depth vanishes, and the behavior of $\lambda_{ab}(T)$ becomes close to that predicted by the isotropic

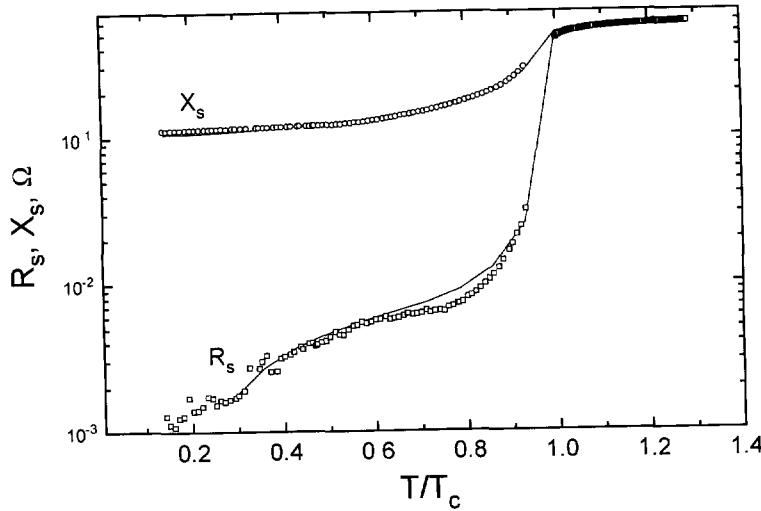


Fig. 8. — Calculated curves ($\gamma_{22}^s = 1.6$ meV, $\gamma_{12} = 0$) compared with data from reference [14] (triangles) and reference [13] (open circles). 1) $\gamma_{22} = 16$ meV, 2) $\gamma_{22} = 32$ meV, 3) $\gamma_{22} = 64$ meV, 4) $\gamma_{22} = 160$ meV. Inset: The crossover from exponential (curves 1,2) to linear (curve 3) behavior of $\Delta\lambda_{ab}(T)$ for $\gamma_{22} = 16$ meV and $\gamma_{22}^s = 0$ (1), 0.8 meV (2) and 3.2 meV (3). Solid squares: data from reference [12].

SC model. Such a crossover illustrated in Figure 1 (and in Fig. 12, see below) correlates with the increase in the resistivity above T_c .

In this paper we generalize these results to describe the c -axis response and to calculate the surface impedance $Z_s(T)$ in the ab -plane of YBCO.

In calculating the ab -plane impedance, we adopt the same assumptions as in our previous work: screening currents are assumed to flow in both subsystems, the intralayer anisotropy is ignored, and the total complex conductivity $\sigma(\omega)$ is calculated in the London (local) limit by the equation $\sigma(\omega) = \alpha\sigma_S(\omega) + \sigma_N(\omega)$, where $\alpha = \nu_S m_N / \nu_N m_S$ ($\nu_{S,N}$ and $m_{S,N}$ are the densities of states and effective masses in the corresponding bands). The temperature dependence of the surface impedance $Z_s(T)$ calculated by the two-band model is shown in Figure 9. The calculations are compared to the experimental data of reference [16] at a frequency $f = 87$ GHz. A reasonable fit of both real and imaginary parts of $Z_s(T)$ is obtained for $\gamma_{22}^s = 0$, and $\gamma_{11} = 6$ meV (solid lines). The real part of the conductivity plotted against temperature, $\sigma_1(T)$ (Fig. 10) is also fitted well by using the same parameters.

Physically the emergence of the maximum in $\sigma_1(T)$ is due to strong temperature-dependent scattering in the N-band. This process can be approximately described as the following sequence of scattering events: N-S-phonon-S-N. *i.e.*, a quasiparticle from the N-band, is scattered to the S-band due to the interband coupling, absorbs a thermal phonon in the S-band and then transfers back to the N-band. This process is strongly temperature dependent due to the strong electron-phonon interaction in the S-band. When the temperature drops below T_c , the scattering rate rapidly decreases and overcompensates the decrease in the quasiparticle number, which is due to gap opening. As a result, the conductivity increases below T_c until at lower temperatures $T < \Delta_N$ the decrease in the quasiparticle number starts to dominate and the conductivity vanishes. Thus the interplay between the T -dependent scattering rate and T -dependent quasiparticle number leads to the emergence of the conductivity maximum. This

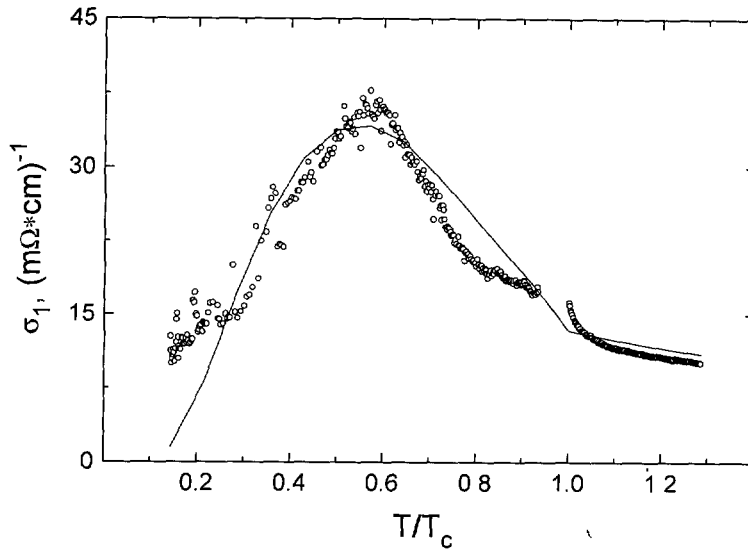


Fig. 9. — Comparison of the temperature dependence of the surface impedance (solid lines) calculated by the two-band model ($\gamma_{22}^s = 0, \gamma_{11} = \gamma_{22} = 6$ meV) with experimental data from reference [16]. Open squares are the real (R_s) and open circles are the imaginary (X_s) parts of the impedance.

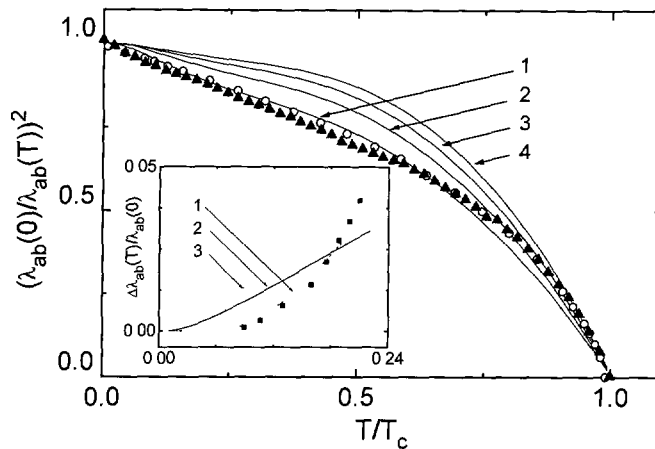


Fig. 10. — Solid line: temperature dependence of the real part of the conductivity σ_1/σ_n calculated by the two-band model with $\gamma_{22}^s = 0, \gamma_{11} = \gamma_{22} = 6$ meV. Open circles: experimental data from reference [16].

mechanism is similar to that discussed for the d-wave model in reference [17], where scattering from low-energy spin fluctuations was considered. An additional physical mechanism, which contributes to the maximum of $\sigma_1(T)$, is the presence of the coherence factors in the N-band since the electron-phonon interaction in this band is weak.

It is interesting to study quantitatively a difference between *ab*- and *c*-axis response for YBCO and to compare it to the predictions of the d-wave pairing model. Anisotropic penetration depth of a layered superconductor consisting of alternating superconducting S and normal N layers

was first calculated by Bulaevskii and Zyskin [34]. Josephson interaction between the layers and a weakly coupled s-wave BCS superconducting state were assumed. Later an essential difference between the c -axis penetration depth $\lambda_c(T)$ behavior predicted by d- and s-pairing models was pointed out in reference [35]. On the other hand, microscopic calculations of the c -axis response in Josephson coupled systems with a single layer type had been done by Graf *et al.* [36]. Later, the consequences of the crossover from direct to impurity assisted tunneling mechanisms of c -axis transport for $\lambda_c(T)$ behavior were discussed by Radtke *et al.* [37] in the similar single layer model. Quite recently, the penetration depth in the ab - and c -directions has been calculated by Atkinson and Carbotte [38] for a layered S/N superconductor in the weak coupling regime, however the impurity scattering and strong-coupling effects have not been included in their formalism.

Here we consider a layered superconductor with two inequivalent layers in the unit cell and study the role of impurity scattering of carriers. We demonstrate that in the direct tunneling regime, the intraplane impurity scattering changes dramatically the temperature dependence of λ_c , and the resulting $\lambda_c(T)$ behavior in the strong scattering limit is quite similar to that in the impurity assisted hopping regime (Josephson coupled regime). Moreover, in all cases there is an essential difference between the curves of the penetration depths in the ab - and c -directions *versus* temperature: the normalized $\lambda_c^2(0)/\lambda_c^2(T)$ curves demonstrate a *weaker* temperature dependence at low T than the corresponding $\lambda_{ab}^2(0)/\lambda_{ab}^2(T)$ curves, in particular, they are never linear in the temperature.

Let us consider the c -axis response in detail. The penetration depth in the coherent regime is given by the expression

$$\lambda_c = \sqrt{4\pi/Q_{\perp}(q=0)}, \quad (9)$$

where the kernel $Q_{\perp}(q=0)$ can be calculated by the generalized technique of reference [26]. The result is

$$Q_{\perp}(q=0) = \frac{e^2}{\pi^2} 2\pi T \int \frac{dS}{|v|} v_z^2 \int d\varepsilon_k \sum_{\omega_n} [G_N(\omega_n)G_S(\omega_n) + F_N(\omega_n)F_S(\omega_n)]. \quad (10)$$

Here the Green's functions $G_{N,S}$ and $F_{N,S}$ are expressed through the solutions of the Eliashberg equations in the following way: $G_N = (i\omega'_{N,n} + \varepsilon_k)/[(\Delta'_{N,n})^2 + (\omega'_{N,n})^2 + \varepsilon_k^2]$, $G_S = (i\omega'_{S,n} + \varepsilon_k)/[(\Delta'_{S,n})^2 + (\omega'_{S,n})^2 + \varepsilon_k^2]$ and $F_N = \Delta'_{N,n}/[(\Delta'_{N,n})^2 + (\omega'_{N,n})^2 + \varepsilon_k^2]$, $F_S = \Delta'_{S,n}/[(\Delta'_{S,n})^2 + (\omega'_{S,n})^2 + \varepsilon_k^2]$. Substituting the expressions for the Green's functions into equation (10) and integrating over the energy ε_k and the Fermi surface dS , we finally obtain the following expression for $\lambda_c(T)$:

$$\lambda_c^{-2}(T) = 2\pi T N(0) e^2 v_z^2 \times \sum_{\omega_n=0}^{\infty} \frac{\Delta_1(i\omega_n)\Delta_2(i\omega_n)}{\sqrt{\omega_n^2 + \Delta_1^2(i\omega_n)}\sqrt{\omega_n^2 + \Delta_2^2(i\omega_n)} \left[\sqrt{\omega_n^2 + \Delta_1^2(i\omega_n)} + \sqrt{\omega_n^2 + \Delta_2^2(i\omega_n)} + \gamma_{11} + \gamma_{22} \right]} \quad (11)$$

Here the Fermi velocity along the c -direction is given by $v_z = W^2 d^2/2$, where W is the hopping integral characterizing the width of the band in the c -axis direction and d is the interlayer distance. According to [39], this approach is valid for sufficiently strong scattering $W < \gamma_{11}, \gamma_{22}$, when both components of the layered-metal conductivity have the Drude form. The vertex corrections are not taken into account in the derivation of equation (11) since they will lead to a renormalization of coupling constants λ_{ij} and scattering rates γ_{ij} and a power-law T -dependence at low temperatures even in an isotropic one-band superconductor [8]. Since we are interested in specific two-band effects, we will not consider these corrections in the paper.

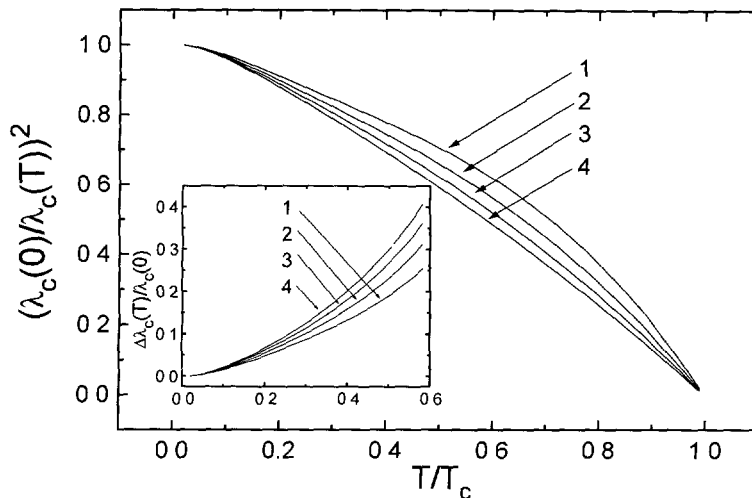


Fig. 11. — Plots of $\lambda_c^{-2}(T)$ vs. T/T_c , calculated by the two-band model with $\gamma_{22}^s = 1.6$ meV. Josephson limit (1), $\gamma_{11} = 8$ meV (2), 2 meV (3), $\gamma_{11} = 0$ meV (4). Inset: Low T portion of $\delta\lambda_c(T)$ vs. T/T_c .

In the final form of equation (11), we have neglected the contribution of the small interband scattering γ_{12}, γ_{21} and magnetic scattering γ_{22}^s . The important parameters which control the shape of the $\lambda_c^{-2}(T)$ curve are the impurity scattering rates γ_{11} and γ_{22} .

The impurity assisted hopping regime can be realized in two ways: (1) for $W \geq \gamma_{11}, \gamma_{22}$ (the clean-limit regime for the c -axis transport), Zener oscillations with rare dephasing events take place, which results in a nonmetallic c -axis conductivity [39]. (2) the interband scattering is strong enough: $W \leq \gamma_{12}, \gamma_{21}$. In this regime, the penetration depth λ_c is determined by the Josephson interaction between neighboring layers and is given by the following expression [30, 34, 36, 37]:

$$\frac{\lambda_c^2(0)}{\lambda_c^2(T)} = 8\gamma^* \frac{T}{T_c} \sum_{\omega_n=0}^{\infty} \frac{\Delta_1(i\omega_n)\Delta_2(i\omega_n)}{\sqrt{\omega_n^2 + \Delta_1^2(i\omega_n)}\sqrt{\omega_n^2 + \Delta_2^2(i\omega_n)}} \quad (12)$$

It is interesting to note that in the strong scattering limit, when $\gamma_{11}/\pi T_c, \gamma_{22}/\pi T_c \gg 1$, one can neglect the terms $\sqrt{\omega_n^2 + \Delta_{1,2}^2(i\omega_n)}$ in the square brackets in the denominator of equation (11) and obtain the T -dependence of $\lambda_c^2(0)/\lambda_c^2(T)$ coinciding with that given by equation (12) for the Josephson coupled regime, although the absolute values of $\lambda_c(0)$ are different in both regimes. This means that a transition from the clean to dirty limit leads to radical changes in $\lambda_c(T)$ similarly to isotropic superconductors. This crossover from clean to dirty limit should be taken into account when discussing the experimental data for c -axis response of layered high T_c superconductors.

Numerical calculations of $\lambda_c(T)$ have been done in the two-band model for the cases of coherent and incoherent transport.

Figure 11 shows the calculations for $\gamma_{22}^s = 1.6$ meV with linear $\lambda_{ab}(T)$ for $T < T_c/2$. The upper curve shows the results in the Josephson (incoherent) regime, whereas the lower curves in the coherent regime for $\gamma_{11} = \gamma_{22} = 0, 2$ and 8 meV. With an increase in γ_{11} and γ_{22} , the crossover from the coherent to the Josephson coupling regime takes place. An increase in the nonmagnetic scattering leads to an increase in the penetration depth at a constant temperature,

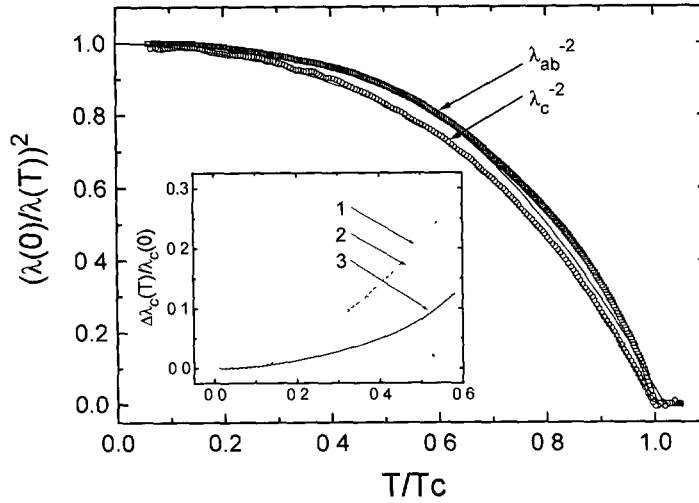


Fig. 12. — $\lambda^{-2}(T)$ vs. T/T_c for $\lambda_c(T)$ and $\lambda_{ab}(T)$ from reference [40]. Solid: two-band model with $\gamma_{22}^s = 6.4$ meV, $\gamma_{12} = 1.6$ meV, $\gamma_{22} = 24$ meV. Inset: Low T section of $\delta\lambda_c(T)$ vs. T/T_c , Josephson limit. Dashed line: $\gamma_{22}^s = 0$ meV, dotted line: $\gamma_{22}^s = 1.6$ meV; solid line: $\gamma_{22}^s = 6.4$ meV.

as a result the curves $\lambda_c^{-2}(T)$ shift upwards and the slope near T_c increases. In contrast to the linear behavior of $\lambda_{ab}^{-2}(T)$ calculated with these parameters at $T < T_c/2$, the T -dependence of $\lambda_c^{-2}(T)$ is power-law, the exponent being only weakly dependent on γ_{11} and γ_{22} .

Figure 12 compares the two-band model for $\gamma_{22}^s = 6.4$ meV and $\gamma_{22} = 24$ meV with the data on c -oriented YBCO powders [40]. An excellent agreement is seen throughout the temperature range for both $\lambda_{ab}(T)$ and $\lambda_c(T)$. The behavior of $\Delta\lambda_c(T)$ of NS multilayer in the Josephson coupling regime is shown in the inset to Figure 12 for different γ_s . It can be seen that $\Delta\lambda_c(T)$ remains nonlinear at low T at all γ_s . The absolute values of λ_c at a given temperature grow with γ_s since the superconductivity in the N-band is destroyed by the pair breaking effect due to magnetic impurities.

5. Conclusion

Measurements of the microwave impedance in Nb, BKBiO, and YBCO have been compared. Our analysis is based on the measurements by the "hot finger" cavity perturbation technique and the theoretical studies in the framework of the s -wave BCS including strong coupling effects (Eliashberg theory), influence of the inhomogeneous broadening of the superconducting transition, and strong interband anisotropy (specific for YBCO).

It is shown that the electromagnetic properties of Nb are in good quantitative agreement with the isotropic s -wave BCS theory. The data for BKBO are also well described by the conventional theory with corrections for the inhomogeneous T_c broadening.

The application of the two-band model to the interpretation of the microwave impedance data of YBCuO reveals a good agreement between theory and experiment for the ab -plane response. The model correctly describes the disappearance of the linear term in $\lambda_{ab}(T)$ with the increase in the sample resistivity, the effect being related to the of impurity scattering. The prediction that a linear term should not appear in $\lambda_c(T)$ is also in accordance with the experiment.

In spite of the good fit, there are some difficulties with the two-band interpretation. First, the two-band model cannot describe the similarity between the penetration depths along a - and b -directions *versus* temperature reported in [41]. The different role of Ni and Zn impurities in YBCO [13] is also not yet clear. The maximum in $\sigma_1(T)$ is naturally explained by this model, but its height of 10-20 (divided by the conductivity above T_c) reported in [13,41] is difficult to reconcile with the parameters chosen for YBCO. That means that further refinement of the model is necessary (one possible modification has been proposed quite recently [42]). On the other hand, the d-wave interpretation is also not free of problems. Therefore one can not make a conclusive choice between s- and d-wave descriptions YBCO on the basis of available microwave measurements, and this issue is beyond the framework of the present paper.

The key experiments to check the two-band description for YBCO could be measurements of $\lambda_c(T)$ on YBCO single crystals, as well as measurements of $\lambda_{ab}(T)$ in Fe- or Ga-doped YBCO, when superconductivity of the CuO chains is destroyed. Another crucial evidence in favor of this model could be measurements of a π -shift in the Josephson effect in YBCO under similar doping [43]. It has been shown above that the two-band scenario is very sensible to the superconductivity in the chain band and therefore predicts a crossover to the conventional behavior under such a doping. In contrast, the generic behavior in the d-wave model is governed by a single CuO plane, and such a crossover is not predicted.

Acknowledgments

We are grateful to G.M. Eliashberg, N. Klein, V.Z. Kresin, E.G. Maksimov, G. Müller, S. Orbach-Werbig, and S. Hensen for useful discussions and communications about their experimental data, and to A.T. Sokolov for technical support. We would like to express our gratitude to the late Prof. I.F. Schegolev for his constant interest to and sponsorship of this research. The work was supported by Russian Foundation for Basic Research under Grant No 94-02-03236 and by HTSC Foundation under Grant No 93194.

References

- [1] Bardeen J., Cooper L.N. and Schrieffer J.R., *Phys. Rev.* **108** (1957) 1175.
- [2] Klein O., Nicol E.J., Holczer K., *et al.*, *Phys. Rev. B* **50** (1994) 6307.
- [3] Eliashberg G.M., *Sov. Phys. JETP* **11** (1960) 696.
- [4] Marsiglio F., *Phys. Rev. B* **44** (1991) 5373.
- [5] Holczer K., Forro L., Myhaly L., *et al.*, *Phys. Rev. Lett.* **67** (1991) 152.
- [6] Golubov A.A., Trunin M.R., Shulga S.V., *et al.*, *Physica C* **213** (1993) 139.
- [7] Anlage S.M., Mao J., Booth J.C., *et al.*, *Phys. Rev. B* **53** (1996) 2792.
- [8] Eliashberg G.M., Klimovich G.V. and Rylyakov A.V., *J. Supercond.* **4** (1991) 393.
- [9] Anlage S.M. and Wu D.-H., *J. Supercond.* **5** (1992) 395.
- [10] Hardy W.N., Bonn D.A., Morgan D.C. *et al.*, *Phys. Rev. Lett.* **70** (1993) 3999.
- [11] Ma Z., Taber R.C., Lombardo L.W. *et al.*, *Phys. Rev. Lett.* **71** (1993) 781.
- [12] Klein N., Tellmann N., Schulz H. *et al.*, *Phys. Rev. Lett.* **71** (1993) 3355.
- [13] Bonn D.A., Kamal S., Zhang Kuan *et al.*, *Phys. Rev. B* **50** (1994) 4051.
- [14] Mao Jian, Wu D.H., Peng J.L. *et al.*, *Phys. Rev. B* **51** (1995) 3316.
- [15] Jacobs T., Sridhar S., Rieck C.T., *et al.*, *J. Phys. Chem. Solids* **56** (1995) 1945.
- [16] Orbach-Werbig S., Golubov A.A., Hensen S. *et al.*, *Physica C* **235-240** (1994) 2383.

- [17] Hirschfeld P.J., Puttka W.O. and Scalapino D.J., *Phys. Rev. B* **50** (1994) 10250.
- [18] Sridhar S. and Kennedy W.L., *Rev. Sci. Instrum.* **54** (1988) 531.
- [19] Trunin M.R., Zhukov A.A. and Sokolov A.T., unpublished.
- [20] Klinkova L.A., Barkovskii N.V., Zver'kov S.A., *et al.*, *Superconductivity* **7** (1994) 1437.
- [21] Jin W., Degani M.H., Kalia R.K., *et al.*, *Phys. Rev. B* **45** (1992) 5535.
- [22] Marsiglio F., Carbotte J.P., Pushkov A., *et al.*, to be published.
- [23] Kosugi M., Akimitsu J., Uchida T., *et al.*, *Physica C* **229** (1994) 389.
- [24] Puchkov A.V., Timusk T., Mosley W.D., *et al.*, *Phys. Rev. B* **50** (1994).
- [25] Affronte M., Marcus J., Escribe-Filippini C., *et al.*, *Phys. Rev. B* **49** (1994) 3502.
- [26] Nam S.B., *Phys. Rev.* **156** (1967) 470, 487.
- [27] Turneaure J.P., Halbritter J. and Schwettman H.A., *J. Supercond.* **4** (1991) 341.
- [28] Pambianchi M.S., Anlage S.M., Hellman E.S., *et al.*, *Appl. Phys. Lett.* **64**(2) (1994) 244.
- [29] Panagopoulos C., Cooper J.R., Peacock G.B., *et al.*, *Phys. Rev. B* **53** (1996) R2999.
- [30] Golubov A.A., Trunin M.R., Zhukov A.A., *et al.*, *JETP Lett.* **62** (1995) 496.
- [31] Kresin V.Z. and Wolf S.A., *Phys. Rev. B* **46** (1992) 6458; **51** (1995) 1229.
- [32] Adrian S.D., Reeves M.E., Wolf S.A., *et al.*, *Phys. Rev. B* **51** (1995) 6800.
- [33] Dolgov O.V. and Shulga S.V., unpublished.
- [34] Bulaevskii L.N. and Zyskin M.V., *Phys. Rev. B* **42** (1990) 10 230.
- [35] Klemm R.A. and Liu S.H., *Phys. Rev. Lett.* **74** (1995) 2343.
- [36] Graf M.J., Rainer D. and Sauls J. A., *Phys. Rev. B* **47** (1993) 12 089.
- [37] Radtke R.J. and Levin K., *Physica C* **250** (1995) 282; Radtke R.J., Kostur V.N. and Levin K., *Phys. Rev. B* **53** (1996) R522.
- [38] Atkinson W.A. and Carbotte J.P., *Phys. Rev. B* **51** (1995) 16 371; **52** (1995) 10 601.
- [39] Varlamov A.A., *Europhys. Lett.* **28** (1994) 347.
- [40] Neminskii A.M. and Nikolaev P.N., *Physica C* **212** (1993) 389.
- [41] Zhang K., Bonn D.A., Kamal S., *et al.*, *Phys. Rev. Lett.* **73** (1994) 2484.
- [42] Combescot R. and Leyronas X., *Phys. Rev. Lett.* **75** (1995) 3732.
- [43] Mazin I.I., Golubov A.A. and Zaikin A.D., *Phys. Rev. Lett.* **75** (1995) 2574.